PCCP

PAPER

View Article Online
View Journal | View Issue

Published on 13 October 2014. Downloaded by National Chiao Tung University on 21/07/2015 11:01:10.

Cite this: *Phys. Chem. Chem. Phys.*, 2014, **16**, 25883

Trajectory-based nonadiabatic molecular dynamics without calculating nonadiabatic coupling in the avoided crossing case: *trans* ↔ *cis* photoisomerization in azobenzene†

Le Yu,[a] Chao Xu,[ab] Yibo Lei,[c] Chaoyuan Zhu*[a] and Zhenyi Wen[c]

Received 6th August 2014,
Accepted 13th October 2014

DOI: 10.1039/c4cp03498h

www.rsc.org/pccp

We develop a novel method to simulate analytical nonadiabatic switching probability based on effective coupling and effective collision energy by using only electronic adiabatic potential energy surfaces and its gradients in the case of avoided crossing types of nonadiabatic transitions. In addition, the present method can keep the same time step for computing both on-the-fly trajectory and nonadiabatic transitions accurately. The present method is most useful for localized nonadiabatic transitions induced by conical intersection. We employ the on-the-fly surface hopping algorithm with an *ab initio* quantum chemistry calculation to demonstrate a dynamic simulation for photoisomerization in azobenzene. Simulated quantum yield and lifetime converge to 0.39 and 53 femtosecond, respectively (0.33 and 0.81 picosecond) for *cis*-to-*trans* (*trans*-to-*cis*) photoisomerization with up to 800 (600) sampling trajectories. The present results agree well with those of the experiment, as well as results simulated with use of nonadiabatic coupling within Tully's fewest switching method. The present trajectory-based nonadiabatic molecular dynamics free from nonadiabatic coupling greatly enhances the simulation power of molecular dynamics for large complex chemical systems.

1. Introduction

Trajectory-based non-Born–Oppenheimer molecular dynamics, one of the most important tools for studying photophysical and photochemical processes for large complex chemical systems,[1] extends the classical trajectory of nuclear motion from an electronic ground-state potential energy surface (PES) to an electronic excited-state PES.[2] The nonadiabatic coupling between two electronic states drives classical trajectory switching from one electronic state to another. The trajectory surface hopping (TSH) method is a stochastic method, which attempts to make the electronic probability distribution averaged over an ensemble of trajectories equal to the probability distribution computed from the electronic density matrix. The TSH methods mostly differ in computing nonadiabatic switch probability, which governs trajectory hopping from one electronic potential energy surface to another. Tully's fewest switching (TFS) trajectory surface hopping[3] provides one of the most successful methods to calculate this switching probability, which is extended to nonadiabatic Car–Parrinello molecular dynamics[4] and nonadiabatic molecular dynamics with time-dependent density functional methods.[5,6] This switching probability is solved by integrating the first-order coupled time-dependent Schrödinger equations involving coupling term $\sum_{i=1}^{N} \dot{\mathbf{R}}_i \cdot \mathbf{d}_{12}^i$ (N is number of nuclei in molecule), in which $\dot{\mathbf{R}}_i$ is the velocity of classical nuclei, and $\mathbf{d}_{12}^i$ is the nonadiabatic coupling vector between two electronic states. Based on the two-state Landau–Zener linear curve crossing model, in which two linear diabatic potential energy curves and constant diabatic coupling are assumed at the avoided crossing point, this switching probability has been formulated in terms of two unitless parameters, namely, effective coupling and effective collision energy,[7]

$$a^2 = \frac{\hbar^2}{2\mu}\frac{\sqrt{|F_2F_1|}|F_2 - F_1|}{(2V_{12})^3} \quad (1)$$

and

$$b^2 = (E_t - E_X)\frac{|F_2 - F_1|}{\sqrt{|F_2F_1|}(2V_{12})}, \quad (2)$$

in which F_1 and F_2 are the forces on two diabatic potential energy surfaces, V_{12} is the diabatic coupling, μ is reduced mass

[a] *Institute of Molecular Science, Department of Applied Chemistry, and Center for Interdisciplinary Molecular Science, National Chiao-Tung University, Hsinchu 300, Taiwan. E-mail: cyzhu@mail.nctu.edu.tw*
[b] *Department of Chemistry, Beijing Normal University, Beijing 100875, P. R. China*
[c] *Institute of Modern Physics, Northwest University, Xi'an, 710069, P. R. China*

† Electronic supplementary information (ESI) available. See DOI: 10.1039/c4cp03498h

Published on 13 October 2014. Downloaded by National Chiao Tung University on 21/07/2015 11:01:10.

of the diatomic molecule, E_X is energy at the crossing point and E_t (see eqn (15)) is the potential energy plus kinetic energy component in the direction of the nonadiabtic coupling vector. Based on these two unitless parameters, Zhu and Nakamura[8,9] developed an improved Landau–Zener formula for switching probability valid up to the nonadiabtic transition region $b^2 \to 0$ expressed as follows:

$$p = \exp\left[-\frac{\pi}{4\sqrt{a^2}}\sqrt{\frac{2}{b^2+\sqrt{|b^4 \pm 1|}}}\right], \quad (3)$$

where + (−) stands for $F_1F_2 > 0$ ($F_1F_2 < 0$). The fewest switching probability is a local nonadiabatic transition probability calculated at each integration time step along a trajectory, and in principle, the trajectory can make an attempted hop at any time. On the other hand, the analytical switching probability in eqn (3) is a global switching probability calculated at an avoided crossing point, and it represents an averaged nonadiabatic transition probability along a trajectory. The trajectory surface hopping is actually carried out when this switching probability is greater than a uniform random number generated between 0 and 1. For systems in which nonadiabatic transitions occur dominantly at avoided crossing zones, two switching probabilities should lead to the same results. Actually, this analytical switching probability has been applied to the charge transfer reaction in the DH_2^+ system, and calculated cumulative reaction probabilities and cross sections are in good agreement with exact quantum mechanical calculations.[10,11] However, it requires a predetermining seam surface between two adiabatic potential energy surfaces instead of calculating the nonadiabatic coupling vector. It is difficult to apply this analytical switching probability to more than a three-atom system due to the difficulty of searching seam surfaces. By approximately estimating the direction of nonadiabatic coupling vector, this switching probability has been applied to large systems where nonadiabatic transitions occur at localized conical intersection zones, and it works well in comparison with experimental results; these were demonstrated in dihydrodibenzodiazocine photoisomerization[12] and on-the-fly nonadiabatic dynamics for the retinal Schiff base.[13] Either predetermining seam surfaces or calculating a nonadiabatic coupling vector restricts this analytical switching probability applied to large complex chemical and physical systems.

Here, we report a novel approach for generalizing two parameters in eqn (1) and (2) along time-dependent classical trajectories based on only adiabatic potential energy surfaces and its gradients in the case that nonadiabatic transitions occur in avoided crossing zones. This makes the present method almost as simple as molecular dynamics on a single potential energy surface.

Nonadiabatic transitions through conical intersections play a significant role in many photochemical and photophysical processes.[14] Conical intersections exhibit localized characterization of nonadiabatic transitions, such that simulated trajectory may make surface hopping mostly appear in the local region of avoided crossing zones. This makes for an ideal case to demonstrate trajectory-based nonadiabatic molecular dynamics work with the analytical switching probability. There are many examples of photochemical isomerisations to involve conical intersections, and *cis*-to-*trans* and *trans*-to-*cis* azobenzene photoisomerization as a prototype has been extensively studied, both theoretically[15–22] and experimentally [ref. 23 and references therein]. In particular, it is worth mentioning that without calculating the nonadiabatic coupling vector, the switching probability $p = \kappa \exp[-\chi|\Delta V_{12}|]$ has been applied to study azobenzene photoisomerization,[21,22] in which κ and χ are fitting parameters. It is interesting to compare with the present form in eqn (3) that takes the form of $p \propto \exp[-\chi(\Delta V_{12})^2]$.

We employ on-the-fly trajectory surface hopping algorithm to study both *cis*-to-*trans* and *trans*-to-*cis* azobenzene photoisomerization. The adiabatic ground-state and the first excited-state potential energy surfaces and its gradients are calculated by a state-averaged, completely active space self-consistent field (SA-CASSCF) method with basis set 6-31G. The analytical switching probability is calculated on the fly along the trajectory. We report simulated quantum yields and lifetimes for *cis*-to-*trans* with 800 sampling trajectories and for *trans*-to-*cis* with 600 sampling trajectories. We make an extensive comparison with the previous calculations based on TFS nonadiabatic switching probabilities.

The rest of this study is organized as follows: Section 2 introduces the present algorithm to generalize the multidimensional form of the effective coupling and the effective collision energy, as well as the hopping direction based only on adiabatic potential energy surfaces and its gradients. Section 3 applies the present method to photoisomerization in azobenzene and shows why the SA2-CAS(6,6)/6-31G method is adequate for running on-the-fly nonadiabatic molecular dynamics for azobenzene. Section 4 presents extensive comparisons with results calculated by Tully's fewest switching probability and by the energy-gap switching probability. Concluding remarks are mentioned in Section 5.

2. The new algorithm of diabatization at avoided crossing zones

The nuclear coordinates and velocities in Cartesian coordinates are propagated along on-the-fly classical trajectories by numerically integrating the Newtonian equation of motion with the velocity-Verlet method.[24] From three consecutive time steps, shown in Fig. 1(a), in which the minimum adiabatic potential gap is assumed to be detected, we convert multidimensional forces into one-dimensional forces in eqn (1) and (2) along a trajectory,

$$\frac{|F_2 - F_1|}{\sqrt{\mu}} = \sqrt{\sum_{i=1}^{N}\frac{1}{m_i}\sum_{\alpha=x,y,z}\left(F_2^{i\alpha} - F_1^{i\alpha}\right)^2}, \quad (4)$$

and

$$\frac{\sqrt{|F_2F_1|}}{\sqrt{\mu}} = \sqrt{\left|\sum_{i=1}^{N}\frac{1}{m_i}\sum_{\alpha=x,y,z}F_2^{i\alpha}F_1^{i\alpha}\right|}, \quad (5)$$

where N is number of nuclei in molecule with the mass m_i (i = 1, 2,..., N), and multidimensional diabatic forces are given as

$$F_1^{i\alpha} = -\frac{\partial V_1}{\partial R_{i\alpha}} \quad \text{and} \quad F_2^{i\alpha} = -\frac{\partial V_2}{\partial R_{i\alpha}}, \quad (6)$$

 This journal is © the Owner Societies 2014

Published on 13 October 2014. Downloaded by National Chiao Tung University on 21/07/2015 11:01:10.

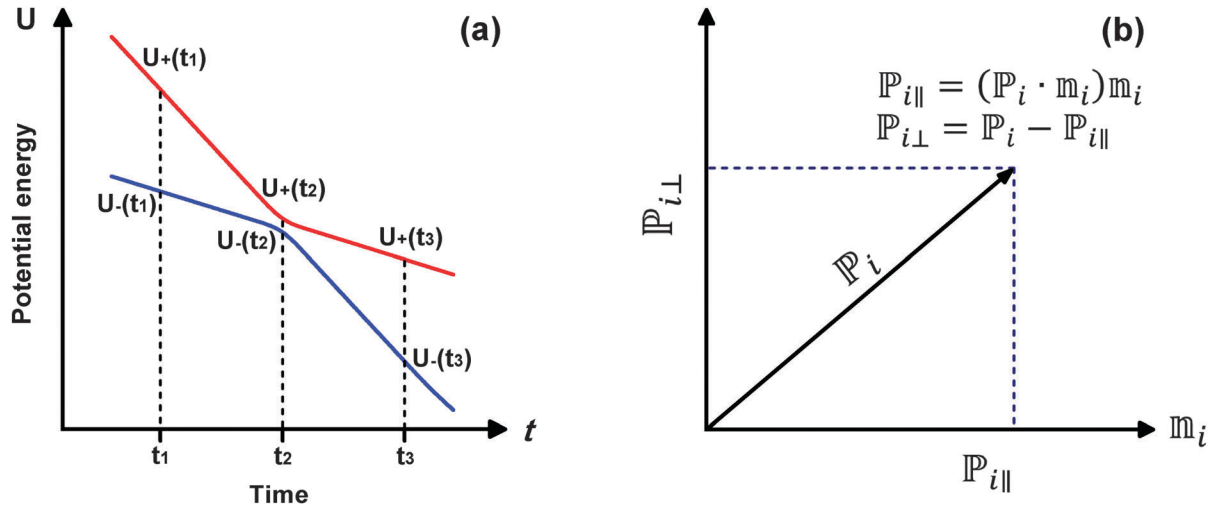

Fig. 1 Hopping scheme along trajectory. (a) Hopping point (t_2) at minimum energy separation between two adiabatic potential energy surfaces. (b) Classical momentum decomposition, according to hopping direction $\mathbf{n}_i$.

in which $R_{i\alpha}$ stands for the x, y, and z components of the Cartesian coordinates for the ith nucleus. It is easy to prove that eqn (4) and (5) return to their original forms if a diatomic molecule is applied. In the case of a conical intersection, the regularized diabatic states[25] can be defined, by which we could generalize a one-dimensional Landau–Zener avoided crossing along a curved coordinate of a trajectory in the form of eqn (4), and detailed derivation is given in Appendix A.

Subsequently, we generalize diabatic forces in eqn (6) from two adiabatic potential energy gradients along a trajectory, and we simply make one linear connection of an upper adiabatic force at t_1 with a lower adiabatic force at t_3, and another linear connection of a lower adiabatic force at t_1 with an upper adiabatic force at t_3 (see Fig. 1(a)), namely,

$$F_1^{i\alpha}(t) = -\frac{\partial V_1}{\partial R_{i\alpha}(t)} = \frac{-1}{R_{i\alpha}(t_3) - R_{i\alpha}(t_1)} \times \left[\frac{\partial U_-}{\partial R_{i\alpha}(t_3)}(R_{i\alpha}(t) - R_{i\alpha}(t_1)) - \frac{\partial U_+}{\partial R_{i\alpha}(t_1)}(R_{i\alpha}(t) - R_{i\alpha}(t_3))\right] \quad (7)$$

and

$$F_2^{i\alpha}(t) = -\frac{\partial V_2}{\partial R_{i\alpha}(t)} = \frac{-1}{R_{i\alpha}(t_3) - R_{i\alpha}(t_1)} \times \left[\frac{\partial U_+}{\partial R_{i\alpha}(t_3)}(R_{i\alpha}(t) - R_{i\alpha}(t_1)) - \frac{\partial U_-}{\partial R_{i\alpha}(t_1)}(R_{i\alpha}(t) - R_{i\alpha}(t_3))\right] \quad (8)$$

for $t_1 < t < t_3$, in which U_+ and U_- are the adiabatic potential energy surfaces along a trajectory. Diabatic coupling in eqn (2) is generalized by $2V_{12}(t) = U_+(t) - U_-(t)$. Finally, we get two effective parameters in eqn (1) and (2) at time $t = t_2$ along a trajectory based on only two adiabatic potential energy surfaces and its gradients. It should be noticed that the integration time step should be small enough to maintain good linear approximation of potential energy surfaces in order to have accurate diabatic forces in eqn (7) and (8). The present fitting scheme of the diabatic forces is consistent with the velocity-Verlet method for on-the-fly trajectory calculation, in which the forces within the integration time step are considered as approximately constant. Once the time step is small enough to converge calculation for on-the-fly trajectory, it converges multidimensional diabatic forces in eqn (7) and (8). There is no additional time step requirement for nonadiabatic transitions. This is different from applying TFS switching probability, in which the time step for computing accurate nonadiabatic transitions is considerably smaller than the time step for computing accurate velocity Verlet trajectory.

Another question is how to define trajectory hopping direction for classical nuclear moment. Actually, the nonadiabatic coupling term $\sum_{i=1}^{N} \dot{\mathbf{R}}_i \cdot \mathbf{d}_{12}^i$ indicates that hopping direction should be in the direction of the nonadiabatic coupling vector because this direction has maximum nonadiabatic transition probability. Following this idea, we define a self-consistent hopping direction by the following vector, expressed as:

$$s_{i\alpha} = \frac{F_2^{i\alpha} - F_1^{i\alpha}}{\sqrt{m_i}} \quad (9)$$

with a normalized vector as

$$\mathbf{n}_i = \frac{1}{\sqrt{s_{ix}^2 + s_{iy}^2 + s_{iz}^2}}(s_{ix}, s_{iy}, s_{iz}). \quad (10)$$

Published on 13 October 2014. Downloaded by National Chiao Tung University on 21/07/2015 11:01:10.

The analytical switching probability in eqn (3) increases with the product of the two parameters defined in eqn (1) and (2) as:

$$a^2b^2 \propto \frac{1}{\mu}\frac{(F_2-F_1)^2}{(V_{12})^4} = \sum_{i=1}^{N}\frac{1}{m_i}\sum_{\alpha=x,y,z}\frac{\left(F_2^{i\alpha}-F_1^{i\alpha}\right)^2}{(V_{12})^4} \geq \sum_{i=1}^{N}\frac{1}{m_i}\sum_{\alpha=x,y,z}\left[\frac{\left(\left(F_2^{i\alpha}-F_1^{i\alpha}\right)n_{i\alpha}{}'\right)}{V_{12}{}^2}\right]^2, \quad (11)$$

in which $\mathbf{n}_i'$ is unit vector in the arbitrary direction, only $\mathbf{n}_i' = \mathbf{n}_i$ leads to the maximum a^2b^2 and in turn, it leads to the maximum nonadiabatic transition probability, which can be seen from the Landau–Zener formula for one passage nonadiabatic transition given by:

$$p = \exp\left[-\frac{\pi}{4\sqrt{a^2b^2}}\right] = \exp\left[-\sqrt{\frac{2\mu\pi^2}{\hbar^2(E_t-E_X)}}\frac{(V_{12})^2}{|F_2-F_1|}\right]. \quad (12)$$

This switching probability depends on a ratio between the adiabatic potential energy gap and force difference at the avoided crossing. It should be emphasized that the hopping direction defined in eqn (10) is not necessary to be the direction of nonadiabatic coupling vector. In principle, the regularized diabatic states introduced by Köppel *et al.*[25] can provide the hopping direction (see eqn (A.8) in Appendix A). However, we propose a simple algorithm for the hopping direction, in which the nonadiabatic switching probability has the maximum at the avoided crossing.

The final task is to set up a relation for classical momentum before and after hopping. We could decompose momentum into parallel and perpendicular directions with respect to hopping direction vector $\mathbf{n}_i$ (Fig. 1(b)), expressed as:

$$\mathbf{P}_{i\parallel} = (\mathbf{P}_i\cdot\mathbf{n}_i)\mathbf{n}_i \quad \text{and} \quad \mathbf{P}_{i\perp} = \mathbf{P}_i - (\mathbf{P}_i\cdot\mathbf{n}_i)\mathbf{n}_i. \quad (13)$$

Momentum component $\mathbf{P}_{i\perp}$ is unchanged before and after hopping, and energy conservation provides another relation for momentum component $\mathbf{P}_{i\parallel}$, namely,

$$\mathbf{P}_{i\perp}(+,t) = \mathbf{P}_{i\perp}(-,t) \quad (14)$$

and

$$E_t = U_+(t) + \sum_{i=1}^{N}\frac{\mathbf{P}_{i\parallel}{}^2(+,t)}{2m_i} = U_-(t) + \sum_{i=1}^{N}\frac{\mathbf{P}_{i\parallel}{}^2(-,t)}{2m_i}, \quad (15)$$

in which $(+,t)$ and $(-,t)$ stand for the momentum components on the upper and lower adiabatic potential energy surfaces, respectively, at time t. The last assumption shows that parallel components of momentum keep direction unchanged before and after hopping, and then a simple scaling factor can be obtained from eqn (15) to determine the magnitude change of parallel components of momentum.

Along an on-the-fly running trajectory, we first determine the minimum potential energy gap at an avoided crossing and then compute the effective coupling parameter a^2 in eqn (1). If a^2 is larger than 1000, the switching probability is set up to unity (diabatic limit), and if a^2 is smaller than 0.001, the switching probability is set up to zero (adiabatic limit). When $1000 > a^2 > 0.001$, the calculation of an attempted hopping with switching probability is actually performed, and it is possible to have multiple hops along a single trajectory. However, in practical simulation, the larger the switching probability, the larger the momentum component along the hopping direction that is perpendicular to the seam line, and thus the trajectory usually moves away from the seam at avoided crossings where hopping is taking place. This has been observed in the present simulation of photoisomerization in azobenzene, in which few trajectories experience multiple back-and-forth switches among a thousand sampling trajectories. We now complete the present new formalism for nonadiabatic molecular dynamics based on only two adiabatic potential energy surfaces and its gradients along a trajectory in the case of an avoided crossing type of nonadiabatic transitions.

3. Application to photoisomerization in azobenzene

The analytical switching probability in the global approach is applied to an on-the-fly surface hopping trajectory for photoisomerization in azobenzene and potential energy surfaces, and its gradients are calculated by an *ab initio* quantum chemistry method at SA2-CAS(6,6)/6-31G level with the Molpro 2009.1 program package.[26]

3.1. Comparison with various CASSCF calculations

The number of average states, number of active electrons and number of active orbitals in the CASSCF method are actually correlated, and various their combinations of should be tested to determine an affordable choice at the CASSCF level for dynamic simulation without losing accuracy for potential energy surfaces. Table 1 presents vertical excitation energies calculated from various SAN-CAS(n,m) methods. The multireference perturbation configuration method (CIPSI)[27] shows the best results in comparison with experimental values.[28] Among all CASSCF methods, SA2-CAS(6,6)/6-31G performs best. If we

Table 1 Vertical excitation energies for *cis*- and *trans*-azobenzene. Various combinations of the number of average states, active electrons and active orbitals are performed and compared in state-averaged CASSCF method

Methods	*cis*-Azobenzene (eV)	*trans*-Azobenzene (eV)
SA2-CAS(6,6)/6-31G (this work)	3.05	2.99
SA2-CAS(14,12)/6-31G*[a]	3.38	3.18
SA3-CAS(6,6)/6-31G (this work)	3.05	3.03
SA3-CAS(10,8)/6-31G*/6-31G[b]	3.36	3.24
SA4-CAS(6,6)/6-31G (this work)	3.09	3.03
SA5-CAS(6,4)/6-31G (this work)	3.16	3.08
SA5-CAS(6,4)/STO-3G[c]	3.78	2.96
CIPSI[d]	2.94	2.81
Expt.[e]	2.92	2.82

[a] Ref. 29. [b] Ref. 19. [c] Ref. 16. [d] Ref. 27: CIPSI calculation for 4 singlet and 2 triplet states. [e] Ref. 28.

 This journal is © the Owner Societies 2014

Published on 13 October 2014. Downloaded by National Chiao Tung University on 21/07/2015 11:01:10.

include the S_2 state, the present SA3-CAS(6,6)/6-31G shows considerably large vertical excitation energies just like those performed by the SA3-CAS(10,8)/6-31G*/6-31G level.[19] The values listed in Table 1 are obtained with three singlet states plus one triplet state in the calculation. The present SA4-CAS(6,6)/6-31G calculation shows slightly worse results in comparison with SA2-CAS(6,6)/6-31G level, and thus it is not necessary to include a more averaged state at the CAS(6,6)/6-31G level. We have done calculations for vertical excitation energies with SA5-CAS(6,4)/6-31G in order to compare with calculations by SA5-CAS(6,4)/STO-3G[16] that present quantum yields and lifetimes for photoisomerization from both *cis*- and *trans*-azobenzene. Actually, the SA2-CAS(14,12)/6-31G* calculation produces poor vertical excitation energies,[29] and this shows that more active space and more active electrons do not perform better than less active space and less active electrons. Finally, we decide to use the SA2-CAS(6,6)/6-31G level to perform the present nonadiabatic molecular dynamics simulations.

3.2. Geometry optimizations and energy profiles

Within an *ab initio* quantum chemistry method at the SA2-CAS(6,6)/6-31G level, we found optimized geometries of *cis*- and *trans*-azobenzene in both the S_0 and S_1 states, three transition states in the S_0 state, one transition state in the S_1 state, and two conical intersections between the S_0 and S_1 states. Atom numbering is given in Fig. 2. Table 2 summarizes important internal coordinates around conical intersections; NN and two CN bond lengths, two NNC bond angles, CNNC and two NNCC dihedral angles for optimized geometries and energies. Optimized geometries of *cis*- and *trans*-azobenzene in the S_0 state agree well with experimental results,[28,30,31] and we obtained optimized geometries for *cis*- and *trans*-azobenzene in the S_1 state as well. Calculated vertical excitation energies 3.05 eV(*cis*) and 2.99 eV(*trans*) are also in good agreement with the experimental values 2.92 eV(*cis*) and 2.82 eV(*trans*). We found three transition states in the S_0 state, which are possible pathways for isomerization in azobenzene, namely, rotation (TS-rot), planar inversion (TS-planar-inv) and the inversion-assisted rotation (TS-inv-rot). We found one transition state corresponding to the rotation pathway (TS-rot) in the S_1 state. We found two conical intersections between the S_0 and S_1 states, namely CI-rot and CI-inv. The energy of CI-inv is 0.42 eV higher than energy of CI-rot and 0.29 eV higher than the energy of *trans*-azobenzene in the S_1 state, as shown in the second column of Table 2. This partly explains why CI-inv is not accessible for dynamic simulation starting from the S_1 state. Full geometry data in the Cartesian coordinates for Table 2 are given in the ESI.†

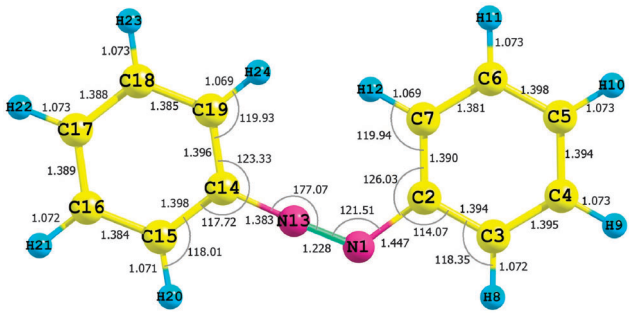

Fig. 2 Atom numbering (geometry of TS-planar-inv in the S_0 state).

Fig. 3 plots energy profiles along the intrinsic reaction coordinate (IRC) based on three transition states, TS-rot, TS-planar-inv, and TS-inv-rot, in the S_0 state. The energy of TS-inv-rot is the lowest, and its structure shows that the two benzene rings are perpendicular to each other. The potential energy curve along IRC in the S_1 state shows a barrier in the *trans*-side and has rather flat region in *cis*-side as shown in Fig. 3(a). The geometry of TS-inv-rot is far from the geometry of two conical intersections, and thus this pathway is unfavorable for photoisomerization in the S_1 state. Although the energy of TS-rot is 0.19 eV higher than the TS-inv-rot in S_0 state, it shows a small energy gap between the S_0 and S_1 states, and its geometry is close to the CI-rot geometry, as shown in Fig. 3(b). Therefore, TS-rot is the most favorable pathway for photoisomerization in the S_1 state. The energy of TS-planar-inv is quite high in the S_0 state, and its geometry is far from both geometries of the conical intersections. In addition, the isomerization following

Table 2 Optimized geometries and energies for equilibriums, transition states, and conical intersections in the ground state S_0 and the first singlet-excited S_1 state. Energies are given in eV. Bond length *r* is given in angstrom (Å), and bond angles *a* and dihedral angles *d* are given in degrees. E_{diff} is the energy gap between S_0 and S_1 states

Geometry	Energy	E_{diff}	r_{NN}	r_{CN}	a_{NNC}	d_{CNNC}	d_{NNCC}
trans S_0	0.00	2.99	1.233	1.422/1.422	117.7/117.7	−180.0	−0.1/−0.1
Expt.[a]		2.82[b]	1.260	1.427/1.427	113.6/113.6	180.0	0.0/0.0
Expt.[c]			1.247	1.428/1.428	113.9/113.9	180.0	0.0/0.0
cis S_0	0.78	3.05	1.231	1.435/1.435	125.9/125.8	−6.4	−52.7/−53.8
Expt.[c]		2.92[b]	1.253	1.449/1.449	121.9/121.9	8.0	53.3/53.3
TS-inv-rot S_0	1.98	1.31	1.210	1.451/1.355	119.2/178.9	−8.5	−1.0/−103.4
TS-rot S_0	2.17	1.00	1.324	1.382/1.382	120.6/120.1	−85.5	−2.7/−2.6
TS-planar-inv S_0	2.21	1.17	1.228	1.447/1.383	121.5/177.1	0.0	0.0/0.0
cis S_1	3.29	1.01	1.213	1.376/1.376	149.2/148.9	0.0	0.0/0.0
trans S_1	2.53	1.95	1.245	1.383/1.383	130.7/130.7	−179.9	0.0/0.0
TS-rot S_1	2.53	0.51	1.244	1.404/1.391	125.5/133.5	−107.9	1.0/8.2
CI-rot S_0/S_1	2.42	0.00	1.244	1.413/1.372	121.8/140.6	−92.6	−0.2/2.7
CI-inv S_0/S_1	2.84	0.00	1.208	1.368/1.296	151.1/154.0	−180.0	0.0/0.0

[a] Ref. 31. [b] Ref. 28. [c] Ref. 30.

Published on 13 October 2014. Downloaded by National Chiao Tung University on 21/07/2015 11:01:10.

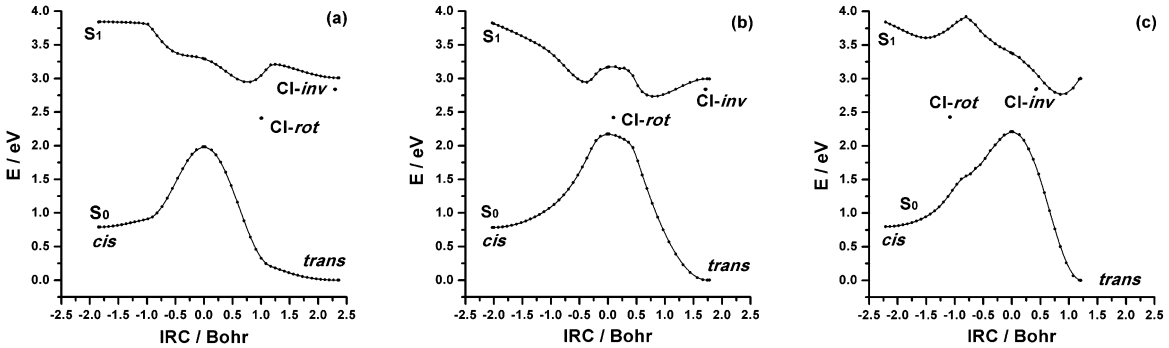

Fig. 3 Potential energy profiles for three transition states in the S_0 state along intrinsic reaction coordinates. (a) Inversion-assisted rotation. (b) Rotation and (c) inversion. The conical intersections between the S_0 and S_1 states, CI-rot and CI-inv, are also plotted for comparison.

this path in the S_1 state is hindered by the large barrier of more than 1.1 eV, which explains why we observe only TS-rot pathway for photoisomerization in the dynamic simulation. We have scanned the two-dimensional potential energy surfaces near the vicinity of the two conical intersections as shown in Fig. S3 of the ESI.†

3.3. Setting up initial and final conditions for trajectory simulation

A canonical ensemble with a temperature of $T = 300$ K is used to specify initial conditions of the trajectories. We first perform frequency calculation at *cis*-azobenzene and *trans*-azobenzene in the S_0 state, where we set up normal-mode velocities with randomly chosen plus or minus sign and then convert them back to velocities in the Cartesian coordinates. The prepared initial coordinates and velocities in the Cartesian coordinates at *cis*-azobenzene and *trans*-azobenzene in the S_0 state are vertically excited to the S_1 state in the Franck–Condon region where trajectory begins evolution. Test runs with time steps of 0.1 fs, 0.25 fs, 0.5 fs, 0.75 fs, and 1 fs are performed to check the robustness of the two parameters defined in eqn (1) and (2), and we, then select the 0.5 fs time step from the beginning to the end of the entire dynamic simulation for trajectory.

The Monte Carlo method is employed to calculate quantum yield with equal weight to all trajectories. Thus, quantum yield is equal to N_r/N, where N is total number of trajectories and N_r is number of reactive trajectories with standard error $\sqrt{(N - N_r)/(NN_r)}$. In total, 800 trajectories have been run starting from *cis*-azobenzene up to 200 fs (trajectories are accounted as resonance if they are still in the S_1 state beyond 200 fs), whereas 600 trajectories have been run starting from *trans*-azobenzene up to 1.5 ps (trajectories are accounted as resonance if they are still in the S_1 state beyond 1.5 ps without the experience of an attempted hopping, otherwise extending to 2.0 ps). There are about 20 percent of resonance trajectories starting from *trans*-azobenzene, and this is because there is a deep potential well around the Franck–Condon region in the S_1 state and trajectories can be trapped there for a long time. On the contrary, there is no resonance trajectory starting from *cis*-azobenzene because there is a very shallow potential well in the Franck–Condon region of the S_1 state, and trajectories go down to the conical intersection very fast.

The isomerization lifetime is estimated by calculating the average population decay in the S_1 state with respect to time evolution and then fitting this decay curve to exponential function $f(t) = \exp[-(t - t_d)/\tau]$, where t_d is the onset time of the S_1 population loss, and τ is the time constant for the exponential decay. The lifetime is estimated as the value of $\tau + t_d$. The error bar of the lifetime is estimated from the fitting procedure. When the number of sampling trajectories is small, the decay curve is not smooth and exhibits a zigzag feature. By fitting the upper and lower bounds of this zigzag curve, we obtain an error estimation of the lifetime. When the decay curve becomes smoother with respect to increased sampling trajectories, this error becomes smaller.

4. Results and discussion

Table 3 shows simulated quantum yields and lifetimes for both *cis*-to-*trans* and *trans*-to-*cis* photoisomerization in comparison with other recent results simulated by the TFS switching probability, the energy gap-dependent empirical switching probability, and the experimental measurements. The present simulated results are in good agreement with the other previous simulations and experimental values to some extent. Simulated quantum yield and the lifetime of *cis*-to-*trans* (*trans*-to-*cis*) converge to 0.39 and 53 fs (0.33 and 0.81 ps) with 800 (600) sampling trajectories as shown in Table 3.

For quantum yield and the lifetime of *cis*-to-*trans*, the present results 0.46 and 54 fs up to 50 sampling trajectories agree with the previous results 0.45 and 60 fs (200 sampling trajectories) simulated by the SA5-CAS(6,4)/STO-3G with the TFS switching probability.[16] For the *trans*-to-*cis* case, the present results 0.30 and 1.0 ps up to 20 sampling trajectories agree with their results 0.28 and 1.86 ps (100 sampling trajectories). It is evident that the present simulation with the analytical switching probability is in rapid convergence, compared with those simulated by the TFS switching probability. Actually, there are two factors to determine the convergence of a non-adiabatic process: one is number of sampling trajectories on a

 This journal is © the Owner Societies 2014

Published on 13 October 2014. Downloaded by National Chiao Tung University on 21/07/2015 11:01:10.

Table 3 Convergence of simulated quantum yields and lifetimes for reactive photoisomerization $S_0 \leftarrow S_1$ in azobenzene with respect to the number of trajectories in comparison with selected simulations and experimental results

		From *cis*-azobenzene		Form *trans*-azobenzene	
	Number of trajectories	Quantum yield	Lifetime (fs)	Quantum yield	Lifetime (ps)
SA2-CAS(6,6)	20	0.50 ± 0.22	55.0 ± 13.3	0.30 ± 0.34	0.97 ± 0.50
	50	0.46 ± 0.15	53.6 ± 8.6	0.30 ± 0.22	1.00 ± 0.30
	100	0.43 ± 0.12	53.8 ± 5.0	0.33 ± 0.14	0.89 ± 0.22
	150	0.43 ± 0.09	53.1 ± 5.0	0.32 ± 0.12	0.88 ± 0.20
	200	0.41 ± 0.08	53.5 ± 4.0	0.34 ± 0.10	0.90 ± 0.15
	300	0.40 ± 0.07	53.4 ± 4.0	0.34 ± 0.08	0.82 ± 0.10
	400	0.40 ± 0.06	52.8 ± 4.0	0.34 ± 0.07	0.80 ± 0.10
	500	0.40 ± 0.06	52.6 ± 4.0	0.34 ± 0.06	0.82 ± 0.10
	600	0.40 ± 0.05	52.6 ± 4.0	0.33 ± 0.05	0.81 ± 0.10
	800	0.39 ± 0.04	53.1 ± 3.0		
TDDFT[a]	400	0.58	121		
OM2/MRCI[b]	920	0.58	72		
SA3-CAS(10,8)[c]	70	0.65 ± 0.11	67		
SA5-CAS(6,4)[d]	200/100	0.45	60	0.28 ± 0.14	1.86
AM1[e]	~200	0.61 ± 0.03	50	0.33 ± 0.03	0.35–0.41
FOCI-AM1[f]	~600	0.49–0.58	70–135	0.24–0.37	0.39–0.54
Force field[g]	1500			0.16–0.52	0.44–5.3
Force field[h]	2000	0.59 ± 0.08		0.11 ± 0.03	
Expt.[i]		0.41–0.56	100–170	0.23–0.35	0.9–1.4

[a] Ref. 20. [b] Ref. 18. (Lifetime is regarded as averaged hopping time.) [c] Ref. 19. [d] Ref. 16. (CH bond constraints with RATTLE algorithms were implemented in simulation.) [e] Ref. 15. [f] Ref. 17. (The solvent effects were represented by the OPLS force field. The quantum yield and lifetimes were obtained by simulations in vacuum, *n*-hexane, methanol and ethylene glycol environments.) [g] Ref. 21. (The quantum yield and lifetimes were obtained by simulations in vacuum, *n*-hexane, toluene, ethanol, anisole and ethylene glycol environments.) [h] Ref. 22. [i] Ref. 23 and references therein.

single adiabatic potential energy surface, and the other is the number of sampling trajectories to simulate nonadiabatic switching probabilities between two adiabatic potential energy surfaces. As mentioned in Tully's original work,[3] in which the TFS switching probability is originated with one-dimensional two-state model systems, in which the convergence is dependent only on the number of trajectories between two potential energy curves; the smaller the switching probability is along the evolution of the trajectory, the more sampling trajectories are required to converge overall nonadiabatic transitions. The TFS switching probability stands for local nonadiabatic transitions and hopping could take place anywhere along one-dimensional, two-state potential energy curves, whereas the present analytical switching probability stands for global nonadiabatic transition, and hopping could take place only at avoided crossings. Therefore, the present method converges faster than the TFS method along this one-dimensional, two-state potential energy curve. However, if a conical intersection has the non-avoided crossing seam or avoided crossing with a higher order than the linear dependence of coordinates with respect to adiabatic potential energy surfaces, the present global approach cannot take into account these nonadiabatic transition regions, whereas the local approach can.

Fig. 4 shows the distribution of successful hopping points with respect to CNNC dihedral angle; the present CNNC dihedral angle is distributed in the range $[-95^\circ,-80^\circ]$ (Fig. 4(a)) in comparison with $[-100^\circ,-70^\circ]$ from ref. 16 for *cis*-to-*trans* isomerization and is distributed in the range $[-105^\circ,-80^\circ]$ (Fig. 4(b)) in comparison with $[-160^\circ,-80^\circ]$ from ref. 16 for *trans*-to-*cis* isomerization. The present and their simulations[16] share a common feature, in which the successful hopping points are taking place mostly in the range of the CNNC dihedral angle larger (smaller) than -92.6° at the conical intersection for *cis*-to-*trans* (*trans*-to-*cis*) isomerization. However, their distributions are very rare in the wide region of the CNNC dihedral angle around the conical intersection, particularly in the *trans*-to-*cis* case. This is because that trajectory takes considerably longer to reach a conical point for the *trans*-to-*cis* case, such that hopping points can be driven everywhere by the TFS switching probability, and many successful hopping points can take place with small TFS switching probabilities. That means considerably more sampling trajectories are needed to converge their calculation for *trans*-to-*cis* isomerization. Their simulations under the condition of frozen all CH bond lengths somehow help convergence with a fewer number of trajectories, otherwise the distribution of the successful hopping points can become even rarer. This is exactly the case for the simulation with a full degree of freedom at the SA3-CAS(8,6)/6-31G level,[19] which presents a quantum yield 0.65 and lifetime 67 fs with up to 70 sampling trajectories for *cis*-to-*trans* isomerization. In general, many hopping trajectories can occur with very small TFS switching probabilities if the trajectories take more time to reach the conical intersection zone, and then convergent overall nonadiabatic transitions must require a large number of sampling trajectories.

The hopping spots in terms of the CNNC dihedral angle are taking place within a 15° (25°) interval by the present global approach in comparison with a 30° (80°) interval by the local approach from ref. 16 for *cis*-to-*trans* (*trans*-to-*cis*) photoisomerization. In the case of *cis*-to-*trans*, the isomerization dynamics are within a short time such that the lifetime is 60 fs with 200 sampling trajectories in the local approach and 53 fs with 800 sampling trajectories in the global approach, compared with the experimental results of 70–100 fs. The two approaches

Published on 13 October 2014. Downloaded by National Chiao Tung University on 21/07/2015 11:01:10.

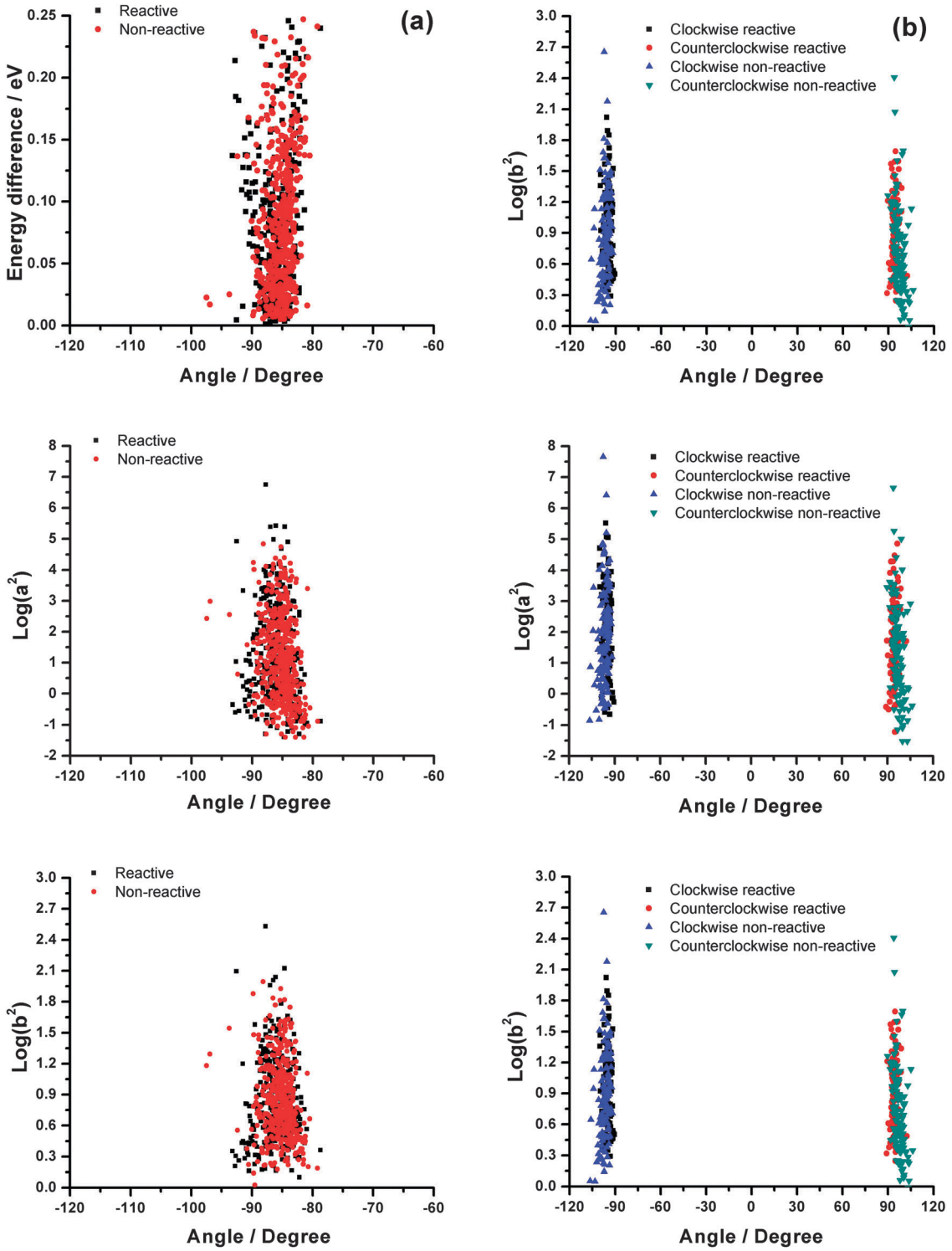

Fig. 4 The distribution of successful hopping points in terms of CNNC dihedral angle. (a) The first panel is for energy gaps, the second panel is for effective coupling parameters, and the third panel is for effective collision energy in the case of *cis*-to-*trans*. (b) The same as (a) but in case of *trans*-to-*cis*.

agree with each other. On the other hand, in the case of *trans*-to-*cis*, the isomerization dynamics are within an extended time such that the lifetime is 1.86 ps with 100 sampling trajectories in the local approach and 0.81 ps with 600 sampling trajectories in the global approach, compared with the experimental results of 0.9–1.4 ps. It appears that the local approach is in one end and the global approach in another. The narrow window of the surface hopping spots in the present global approach directly leads to the short lifetime. Actually, this can also be seen from the force field simulation, in which the lifetime is 0.44 ps with

 This journal is © the Owner Societies 2014

Published on 13 October 2014. Downloaded by National Chiao Tung University on 21/07/2015 11:01:10.

Table 4 The averaged surface hopping time, averaged CNNC dihedral angle and its angle velocity and energy gap at hopping spots for trajectories started from *cis*- and *trans*-azobenzene

	t_{hop} (fs)	d_{CNNC} (deg)	ω_{CNNC}[a] (deg fs^{-1})	ΔE (eV)
cis Reactive counterclockwise	55.3(64.0)	−86.1(−87.1)	−1.80(−2.56)	0.079
cis Non-reactive counterclockwise	50.4(58.1)	−85.3(−87.0)	1.39(0.33)	0.082
trans Reactive clockwise	641.5	−94.7	1.60	0.040
trans Non-reactive clockwise	645.1	−96.8	0.85	0.050
trans Reactive counterclockwise	598.0	94.3	−1.65	0.048
trans Non-reactive counterclockwise	656.4	97.1	1.01	0.072

[a] For the non-reactive trajectories, the angle velocity is obtained as the average of the absolute value of the angle velocity. Numbers in brackets are obtained from ref. 16.

1500 sampling trajectories in terms of semi-empirical energy-gap switching probability[21] and that the effective surface hopping spots are even narrower than the present global approach due to the energy gap in the conical intersection being far apart quickly in terms of the CNNC dihedral angle. However, three approaches present similar results for the quantum yield; they are 0.28, 0.33, and 0.52 in the local, global and energy-gap approaches, respectively, for *trans*-to-*cis* isomerization. In conclusion, the lifetime is more sensitive than the quantum yield in terms of the spots of trajectory hopping distribution. The present global approach can avoid small hopping events resulting in rapid convergence on one hand, but on another hand, it may neglect a certain region where nonadiabatic transitions could accumulate in longtime dynamics. The hopping distribution in energy is around 0 to 0.25 eV (first panel of Fig. 4(a)) in the *cis*-to-*trans* case, whereas around 0 to 0.2 eV in *trans*-to-*cis* case. However, the hopping distribution in the effective coupling parameter a^2 and the effective collision energy b^2 are all in the region of $a^2 \sim [0.1,10^5]$ (second panel of Fig. 4(a, b)) and $b^2 \sim [1,100]$ (third panel of Fig. 4(a, b)) for both *cis*-to-*trans* and *trans*-to-*cis* cases. The present analytical switching probability that represents global nonadiabatic transitions at conical intersection zones (avoided crossing zones) is determined by the distribution of these two dimensionless parameters, and trajectories serve as simulator to decode the distribution of the switching probabilities.

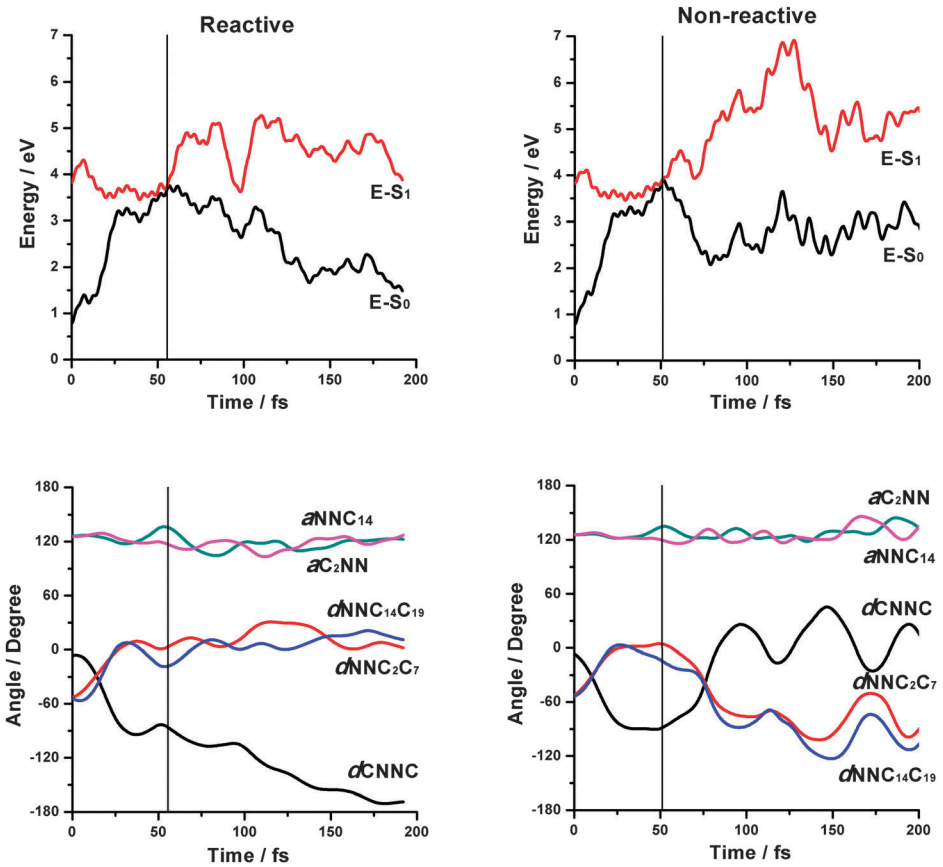

Fig. 5 Potential energies and the five important angles evolve along trajectories starting from *cis*-azobenzene. A typical reactive (left panel) with a^2 = 14.79 and b^2 = 3.52 at a hopping point and a typical non-reactive (right panel) trajectory with a^2 = 75.35 and b^2 = 4.82.

Published on 13 October 2014. Downloaded by National Chiao Tung University on 21/07/2015 11:01:10.

Table 4 shows that the average hopping time starting from *cis*-isomer is 55 fs (50 fs) for reactive (non-reactive) counterclockwise trajectories, which are in good agreement with 64 fs (58 fs) reported from ref. 16. The present average velocity of the CNNC angle at hopping spots is about -1.80 deg fs^{-1} (1.39 deg fs^{-1}) for reactive (non-reactive) counterclockwise rotation trajectories in comparison with -2.56 deg fs^{-1} (0.33 deg fs^{-1}) reported from ref. 16. This difference may come from different initial conditions because we do not observe clockwise rotation starting from the *cis*-isomer. This is understandable from the analysis of the initial condition that can control the rotation of trajectory.[19] The present average energy gap at hopping spots is about 0.08 eV starting from the *cis*-isomer, whereas it is about 0.05 eV starting from the *trans*-isomer. This reflects that a potential energy surface around a conical intersection is not isotropic. Actually starting from the *trans*-isomer, we observe both clockwise and counterclockwise rotation for reactive and nonreactive trajectories, respectively, as shown in Table 4. This is because the *trans*-isomer is almost of planar geometry. The average hopping time at hopping spots from the *trans*-isomer is about 637 fs, which is shorter than the 800 fs reported from ref. 16. The trajectories starting from *trans*-isomers need several hundred femtoseconds to leave the Franck–Condon region, and that leads to long average hopping times and lifetimes. On the other hand, the trajectories starting from *cis*-isomers need several tenths of a femtosecond to leave the Franck–Condon region and then go rapidly toward conical intersection, and this leads to short average hopping times and lifetimes.

There are five highly important angles involving the motion of photoisomerization, which are the two NNC bond angles, the two NNCC and one CNNC dihedral angles, and we plot several typical trajectories in Fig. 5 and 6 to show how these five angles evolves with time along trajectory. A reactive (non-reactive) trajectory starting from the *cis*-isomer takes about 60 fs (50 fs) to hop down to the S_0 state with effective coupling and collision energy parameters a^2 = 14.79 and b^2 = 3.52 (a^2 = 75.35 and b^2 = 4.82) at the hopping point as shown in left (right) panel of Fig. 5. In both reactive and non-reactive cases, the CNNC dihedral angles show the most rapid change, and this indicates that the rotation pathway dominates the isomerization process. The NNCC dihedral angles change in the opposite direction, compared with the CNNC dihedral angle. The two NNC bond angles vibrate slowly until reaching the conical point; one of NNC bond angles increase to about 135°–140°, whereas the other stays around 115°, close to optimized CI-rot structure of 140.6° and 121.8°, respectively. After hopping, the two NNC angles move in opposite directions for both reactive and non-reactive trajectories. The potential energy gap between S_0 and S_1 along both reactive and non-reactive trajectories is rapidly decreasing down to the conical point, and then the energy gap is rapidly far apart toward the product region. This is an indication of rapid isomerization motion for the trajectory starting from the *cis*-isomer. On the other hand, the *trans*-azobenzene has a planar symmetric structure, and thus the trajectories have almost equal opportunity to follow the clockwise and counterclockwise rotation pathways. A clockwise

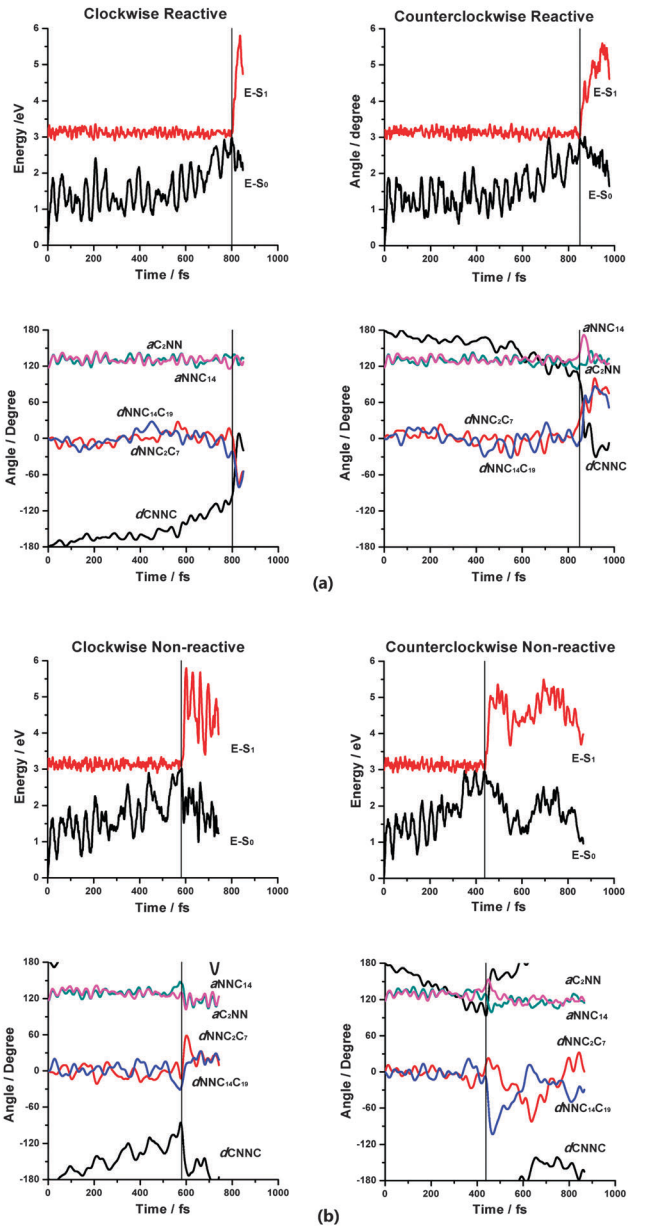

Fig. 6 Potential energies and the five important angles evolve along trajectories starting from *trans*-azobenzene. (a) Typical reactive trajectories; clockwise one (left panel) with a^2 = 0.22 and b^2 = 1.95 and counterclockwise one (right panel) with a^2 = 35.84 and b^2 = 4.26. (b) Typical non-reactive trajectories; clockwise one (left panel) with a^2 = 9.50 and b^2 = 3.07 and counterclockwise one (right panel) with a^2 = 48.17 and b^2 = 6.65.

(counterclockwise) reactive trajectory starting from *trans*-isomer takes about 800 fs (850 fs) to hop down the S_0 state with effective coupling and collision energy parameters a^2 = 0.22 and b^2 = 1.95 (a^2 = 35.84 and b^2 = 4.26) at the hopping point as shown in left (right) panel of Fig. 6(a). A clockwise (counterclockwise) non-reactive trajectory starting from the *trans*-isomer takes about 580 fs (430 fs) to hop down the S_0 state with effective coupling and collision energy parameters a^2 = 9.50 and b^2 = 3.07 (a^2 = 48.17 and b^2 = 6.65) at the hopping point as shown in the left (right) panel of Fig. 6(b). The isomerization

 This journal is © the Owner Societies 2014

Published on 13 October 2014. Downloaded by National Chiao Tung University on 21/07/2015 11:01:10.

process from the *trans*-isomer is considerably slower than that from the *cis*-isomer. Except for the CNNC dihedral angle, the other four angles fluctuate around their initial values along the trajectories. The CNNC dihedral change slowly vibrates around approaching to the conical region with the CNNC dihedral angle ($\sim\pm90^\circ$). In the hopping region, the NNCC dihedral angles move in the opposite direction with respect to the CNNC dihedral angle. The two NNC bond angles separate in the conical region with one of them increases to about 140°, whereas the other decreases to around 120°. We show one typical resonance trajectory in Fig. S1 of the ESI,† in which all five angles vibrate around the initial structure independently, and they never pass through the conical region. We have performed more time propagation up to 3 ps for those resonance trajectories, and they still vibrate on the S_1 potential energy surface. It may need more and more time to bring them down.

We plot population decay from the S_1 state in Fig. 7. Fig. 7(a) shows only one time scale decay from the *cis*-isomer as observed in ref. 16. Fig. 7(b) shows that population decay from the *trans*-isomer has a rapid decay component around 350–450 fs and a slow decay component after 450 fs in the S_1 state, and these two-time-scale decays are also observed by the SA5-CAS(6,4)/STO-3G simulation.[16] We fitted fast and slow motion to exponential functions separately and then average them to have the final lifetime in Table 3.

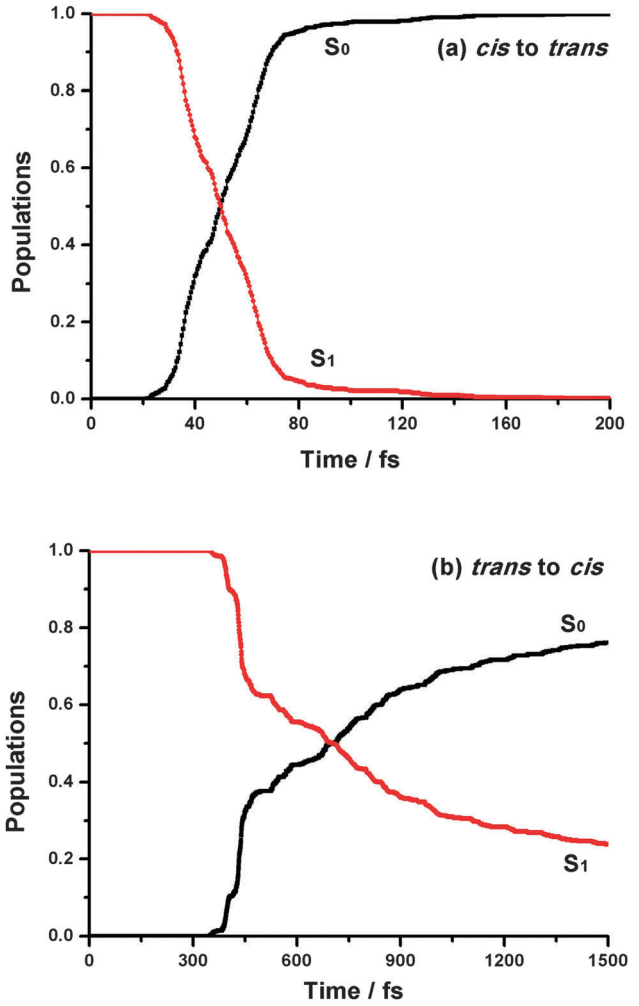

Fig. 7 Average population distribution in the S_1 and S_0 states as a function of time. (a) *cis*-to-*trans* estimated from 800 trajectories. (b) *trans*-to-*cis* estimated from 600 trajectories.

5. Concluding remarks

By generalizing the two unitless parameters (effective coupling constant and effective collision energy) originally for avoiding the crossing type of nonadiabatic transitions in diatomic molecule to multiple-atom molecules, we have accomplished the new algorithm to calculate on-the-fly switching probabilities along a trajectory based on only two adiabatic potential energy surfaces and its gradients. The method is simple and accurate for application in the case of localized nonadiabatic transitions induced by conical intersections. Simply speaking, if one can perform trajectory-based molecular dynamics on a single electronic adiabatic potential energy surface the one can also perform trajectory based non-Born–Oppenheimer molecular dynamics on excited electronic adiabatic potential energy surfaces. This is also potentially useful for force field excited-state molecular dynamic simulation, and it requires force fields only for electronic adiabatic potential energy surfaces.

Incorporating with on-the-fly trajectory surface hopping algorithm, we have applied the present new method to compute analytical switching probabilities and then to simulate azobenzene photoisomerization for both *cis*-to-*trans* (800 sampling trajectories) and *trans*-to-*cis* (600 sampling trajectories) at the SA2-CASSCF(6,6)/6-31G quantum chemistry level. An extensive comparison has been made with the previous simulations performed by Tully's fewest switching method. Quantum yield and lifetime simulated with the present method basically agree with those simulated with the TFS method. The average surface hopping time from the *cis*-isomer (*trans*-isomer) is about 53 fs (637 fs) simulated from the present method in comparison with 50 fs (800 fs) simulated by the TFS method. The present method requires fewer numbers of sampling trajectories to converge overall nonadiabatic switching probabilities than those from the TFS method. However, the present method takes into account a narrower region of nonadiabatic transition zones than the TFS method, and it may result in a certain inaccuracy for more detailed mechanistic aspects such as state-to-state molecular dynamics.

The present method can maintain the same time step for computing both accurate velocity-Verlet trajectories and accurate nonadiabatic transitions, whereas in the TFS switching method time step for computing accurate nonadiabatic transitions is considerably smaller than time steps for computing accurate velocity-Verlet trajectories.

The TFS switching method can deal with not only avoiding crossing types of nonadiabatic transitions, but also non-avoided crossing types of transitions. In general, there are three independent quantities at nonadiabatic transition zones: two adiabatic potential energy surfaces and one nonadiabatic coupling. In the present

Published on 13 October 2014. Downloaded by National Chiao Tung University on 21/07/2015 11:01:10.

method, we need only two adiabatic potential energy surfaces, and this is due to avoiding crossing types of nonadiabatic transition, in which the Landau–Zener type of switching probability includes contribution of nonadiabatic coupling already. In general, we need the rotation angle to transform potential energy surfaces from adiabatic to diabatic representation, and this rotation angle $\theta(R)$ is in the range of zero to $\pi/4$ degree in which $\theta(R) = \pi/4$ represents the maximal mixing of the two representations regarded as the Landau–Zener type of nonadiabatic transitions.[32] The analytical switching probability, including this rotation angle, is formulated for general two-state nonadiabatic transition (including both avoided and non-avoided types of nonadiabatic transitions).[33] It is a very challenging task to generalize this rotation angle in general along on-the-fly trajectory without calculating nonadiabatic coupling. The present study is focusing on avoided crossing types of nonadiabatic transitions, and it is demonstrated to work well for conical intersection types of nonadiabatic transitions in azobenzene photoisomerizations. We will report the other simulations of photoisomerizations with two or more excited states calculated by an *ab initio* quantum chemistry method associated with the present global approach of switching probabilities in the near future.

Appendix A: convert multidimensional conical intersection to one-dimensional avoided crossing along a trajectory

It is known at the crossing point of a conical intersection that the nonadiabatic coupling vector has a removable singularity with a pole of the order 1, and thus a good behavior function of the electronic diabatic potential energy surfaces can be defined. Following the regularized diabatic states introduced by Köppel *et al.*,[25] the diabatic potential energy surfaces can be written in the following form:

$$\mathbf{W}_{\mathrm{reg}} = \begin{pmatrix} \dfrac{U_+ + U_-}{2} & 0 \\ 0 & \dfrac{U_+ + U_-}{2} \end{pmatrix} + \begin{pmatrix} \sum_{i=1}^{N} \kappa_i Q_i & \sum_{j=1}^{M} \lambda_j Q_j \\ \sum_{j=1}^{M} \lambda_j Q_j & -\sum_{i=1}^{N} \kappa_i Q_i \end{pmatrix}, \tag{A.1}$$

where U_+ and U_- are upper and lower *ab initio* adiabatic potential energy surfaces, respectively, and the coupling terms are given by

$$\kappa_i = \frac{1}{2}\left(\frac{\partial U_+}{\partial Q_i} - \frac{\partial U_-}{\partial Q_i}\right)\Bigg|_{\mathbf{Q}=0} \quad \text{and} \quad \lambda_j = \frac{1}{2}\left(\frac{\partial U_+}{\partial Q_j} - \frac{\partial U_-}{\partial Q_j}\right)\Bigg|_{\mathbf{Q}=0}, \tag{A.2}$$

where the crossing point is assumed at multidimensional coordinates $Q_1 = Q_2 = \cdots = 0$ ($\mathbf{Q} = 0$) and eqn (A.1) is valid in the neighborhood of the crossing point. Moreover, we can compute the gap of two adiabatic potential energy surfaces as follows:

$$\Delta V = \sqrt{\left(2\sum_{i=1}^{N} \kappa_i Q_i\right)^2 + 4\left(\sum_{j=1}^{M} \lambda_j Q_j\right)^2}. \tag{A.3}$$

Assume that a multidimensional trajectory can be expressed in terms of a one-dimensional curved coordinate s, and thus we have $Q_i = Q_i(s)$. It is the trajectory that passes through the crossing region and reaches the point $s_0 = s(t_0)$ at time t_0, where the potential gap is the minimum. We expand coordinate Q_i around s_0 as follows:

$$Q_i(s) = Q_i(s_0) + \left.\frac{\mathrm{d}Q_i}{\mathrm{d}s}\right|_{s=s_0} (s - s_0). \tag{A.4}$$

Inserting eqn (A.4) into eqn (A.3) leads to

$$\Delta V = \sqrt{(F_1 - F_2)^2 (s - s_0)^2 + 4(V_{12})^2}, \tag{A.5}$$

in which (at $s = s_0$, the gap is minimum so that the term with $(s - s_0)$ vanishes in eqn (A.5))

$$(F_2 - F_1)^2 = 4\sum_{i,\alpha=1}^{N} \kappa_i \kappa_\alpha \left(\frac{\mathrm{d}Q_i}{\mathrm{d}s}\right)_{s0} \left(\frac{\mathrm{d}Q_\alpha}{\mathrm{d}s}\right)_{s0} + 4\sum_{j,\beta=1}^{M} \lambda_j \lambda_\beta \left(\frac{\mathrm{d}Q_j}{\mathrm{d}s}\right)_{s0} \left(\frac{\mathrm{d}Q_\beta}{\mathrm{d}s}\right)_{s0} \tag{A.6}$$

and

$$(V_{12})^2 = \sum_{i,\alpha=1}^{N} \kappa_i \kappa_\alpha Q_i(s_0) Q_\alpha(s_0) + \sum_{j,\beta=1}^{M} \lambda_j \lambda_\beta Q_j(s_0) Q_\beta(s_0). \tag{A.7}$$

By introducing coordinate transformation $Q_i \rightarrow Q_i'$, we finally reach

$$(F_2 - F_1)^2 = 4\sum_{i=1}^{N} \kappa_i'^2 \left(\frac{\mathrm{d}Q_i'}{\mathrm{d}s}\right)_{s0}^2 + 4\sum_{j=1}^{M} \lambda_i'^2 \left(\frac{\mathrm{d}Q_j'}{\mathrm{d}s}\right)_{s0}^2 \rightarrow \sum_{l=1}^{3n} \left[\left(F_{2l}' - F_{1l}'\right) n_l'\right]^2 \tag{A.8}$$

and

$$(V_{12})^2 = \sum_{i=1}^{N} \kappa_i'^2 Q_i'(s_0)^2 + \sum_{j=1}^{M} \lambda_j'^2 Q_j'(s_0)^2 \rightarrow \left(V_{12}'(s_0)\right)^2. \tag{A.9}$$

Eqn (A.5) shows one-dimensional, two-state Landau–Zener avoided crossing along the curved coordinate and eqn (A.8) is consistent with the present new algorithm eqn (11) in the text. The hopping direction n_l' in eqn (A.8) is selected to provide the maximum switching probability.

Acknowledgements

This work is supported by the Ministry of Science and Technology of the Republic of China under grant no. 100-2113-M-009-005-MY3 and 103-2113-M-009-007-MY3. L. Y. thanks support from the Postdoctoral Fellowship by the Ministry of Science and

 This journal is © the Owner Societies 2014

Published on 13 October 2014. Downloaded by National Chiao Tung University on 21/07/2015 11:01:10.

Technology of the Republic of China under grant no. 102-2811-M-009-044 and 103-2811-M-009-048. C. X. thanks support from visiting student fellowship by the National Chiao Tung University. C. Z. thanks the MOE-ATU project of the National Chiao Tung University for support.

References

1 B. F. E. Curchod, U. Rothlisberger and I. Tavernelli, *ChemPhysChem*, 2013, **14**, 1314–1340.
2 D. Marx and J. Hutter, *Ab Initio Molecular Dynamics: Basic Theory and Advanced Methods*, Cambridge University Press, Cambridge, 2009.
3 J. C. Tully, *J. Chem. Phys.*, 1990, **93**, 1061–1071.
4 N. L. Doltsinis and D. Marx, *Phys. Rev. Lett.*, 2002, **88**, 166402.
5 C. F. Craig, W. R. Duncan and O. V. Prezhdo, *Phys. Rev. Lett.*, 2005, **95**, 163001.
6 E. Tapavicza, I. Tavernelli and U. Rothlisberger, *Phys. Rev. Lett.*, 2007, **98**, 023001.
7 M. S. Child, *Molecular Collision Theory*, Academic, London, New York, 1974.
8 C. Zhu and H. Nakamura, *J. Chem. Phys.*, 1992, **97**, 8497–8514.
9 C. Zhu and H. Nakamura, *J. Chem. Phys.*, 1993, **98**, 6208–6222.
10 C. Zhu, H. Kamisaka and H. Nakamura, *J. Chem. Phys.*, 2002, **116**, 3234–3247.
11 K.-L. Han and B. Li, *J. Chem. Phys.*, 2008, **128**, 114116.
12 A.-H. Gao, B. Li, P.-Y. Zhang and K.-L. Han, *J. Chem. Phys.*, 2012, **137**, 204305.
13 T. Ishida, S. Nanbu and H. Nakamura, *J. Phys. Chem. A*, 2008, **113**, 4356–4366.
14 *Conical Intersections: Electronic Structure, Dynamics & Spectroscopy*, ed. W. Domcke, D. R. Yarkony and H. Köppel, World Scientific, Singapore, 2004.
15 C. Ciminelli, G. Granucci and M. Persico, *Chem. – Eur. J.*, 2004, **10**, 2327–2341.
16 Y. Ootani, K. Satoh, A. Nakayama, T. Noro and T. Taketsugu, *J. Chem. Phys.*, 2009, **131**, 194306.
17 T. Cusati, G. Granucci and M. Persico, *J. Am. Chem. Soc.*, 2011, **133**, 5109–5123.
18 O. Weingart, Z. Lan, A. Koslowski and W. Thiel, *J. Phys. Chem. Lett.*, 2011, **2**, 1506–1509.
19 M. Pederzoli, J. Pittner, M. Barbatti and H. Lischka, *J. Phys. Chem. A*, 2011, **115**, 11136–11143.
20 A. J. Neukirch, L. C. Shamberger, E. Abad, B. J. Haycock, H. Wang, J. Ortega, O. V. Prezhdo and J. P. Lewis, *J. Chem. Theory Comput.*, 2014, **10**, 14–23.
21 G. Tiberio, L. Muccioli, R. Berardi and C. Zannoni, *ChemPhysChem*, 2010, **11**, 1018–1028.
22 Y. Li and B. Hartke, *J. Chem. Phys.*, 2013, **139**, 224303.
23 H. M. Bandara and S. C. Burdette, *Chem. Soc. Rev.*, 2012, **41**, 1809–1820.
24 L. Verlet, *Phys. Rev.*, 1967, **159**, 98–103.
25 H. Köppel, J. Gronki and S. Mahapatra, *J. Chem. Phys.*, 2001, **115**, 2377–2388.
26 MOLPRO, a package of *ab initio* programs written by H.-J. Werner and P. J. Knowles, version 2009.1, G. Knizia, F. R. Manby, M. Schütz, *et al*.
27 P. Cattaneo and M. Persico, *Phys. Chem. Chem. Phys.*, 1999, **1**, 4739–4743.
28 D. L. Beveridge and H. H. Jaffe, *J. Am. Chem. Soc.*, 1966, **88**, 1948–1953.
29 A. Cembran, F. Bernardi, M. Garavelli, L. Gagliardi and G. Orlandi, *J. Am. Chem. Soc.*, 2004, **126**, 3234–3243.
30 J. A. Bouwstra, A. Schouten and J. Kroon, *Acta Crystallogr., Sect. C: Cryst. Struct. Commun.*, 1983, **39**, 1121–1123.
31 T. Tsuji, H. Takashima, H. Takeuchi, T. Egawa and S. Konaka, *J. Phys. Chem. A*, 2001, **105**, 9347–9353.
32 C. Zhu, *Phys. Scr.*, 2009, **80**, 048114.
33 C. Zhu, *J. Chem. Phys.*, 1996, **105**, 4159–4172.